# Development of Strain-Rate-Dependent Material Model for Predicting Tibia Response in Pedestrian-Vehicle Collisions

Ankit Malik[1], Anoop Chawla[1], and Naresh V. Datla[1]
[1] Department of Mechanical Engineering, Indian Institute of Technology Delhi, New Delhi, India

## ABSTRACT

*Lower leg trauma, particularly to the tibia, is common in pedestrian-vehicle collisions and can lead to long-term disability and socioeconomic burden. Accurate finite element (FE) models can help understand the tibia's mechanical response under pedestrian-vehicle impact scenarios, which is crucial for developing effective safety measures and enhancing pedestrian protection. Previous material models considered bone as homogeneous, lacking subject-specific anatomical geometry and material property assignment, and depended solely on yield stress scaling to incorporate the strain-rate effect of bone. This work aims to develop a strain-rate-dependent material model for the human tibia that incorporates subject-specific anatomical geometry and material properties while capturing strain-rate sensitivity in pre- and post-yield regions. Dynamic three-point bending tests were performed on the human tibia at impact velocities of 1.5, 3.0, and 5.0 m/s in the lateral-medial direction at its midshaft. Subject-specific finite element (SSFE) models were created using CT scans, and heterogeneous material properties were mapped based on Hounsfield numbers. A user-defined material model in LS-DYNA™ was used to implement a bilinear isotropic elastic-plastic material model that incorporated the strain-rate dependency of yielding and the pre- and post-yield behavior of bone. The material model parameters were optimized using a genetic algorithm-based inverse FE characterization approach to minimize errors between the experimental and FE force-time responses. The developed FE model reasonably predicts the structural response in all cases, with a summation of normalized root mean square error of 0.285. While the model captures key aspects of tibial behavior, its assumptions of isotropy, symmetric yielding, and exclusion of viscoelasticity might be the possible reason for this error. These limitations and the need for additional experimental repetitions to enhance model reliability will be addressed in future work.*

## INTRODUCTION

Pedestrians are considered a highly vulnerable and high-risk category of road users due to their lack of protection in vehicle collisions. The Global Status Report on Road Safety 2023 (WHO, 2023) indicates that pedestrians constitute 21% of global road deaths. These injuries result in a significant economic burden on society, estimated between 1% and 3% of Gross Domestic Product (GDP) and, in some instances, as high as 6%. The lower leg trauma occurs most frequently



*This paper is a student paper from the 20th Injury Biomechanics Symposium and is published in a special issue of SAE International Journal of Transportation Safety.*
*It is preliminary work, has not been peer reviewed, and should not be cited because it is a work in progress.*

during pedestrian-vehicle collisions (Mo et al., 2012). Despite being infrequently fatal, numerous studies indicate that lower limb injuries lead to substantial healthcare expenses for victims and diminished working productivity (Singaram et al., 2019). The tibia, being the most frequently fractured long bone in such incidents, is especially susceptible to lateral blunt impacts with vehicle bumpers (Yang, 2005). Therefore, understanding the tibia's mechanical behavior under real-world impact scenarios is essential for designing effective injury countermeasures for vehicles and improving pedestrian protection.

Finite element (FE) models offer new perspectives and are essential for understanding the dynamic response of bone under different impact scenarios (Abdel-Wahab et al., 2011; Fleps et al., 2019). However, the accuracy of such FE simulations is significantly dependent on anatomically accurate geometries, representative material models, and appropriate material property assignment to predict the organ-level response effectively. Bone tissue exhibits strain-rate-dependent mechanical behavior due to its complex hierarchical microstructure (Abraham et al., 2016; Hansen et al., 2008). An elastic-plastic material model with the Cowper–Symonds formulation is commonly used to capture bone strain-rate effects (Asgharpour et al., 2014; Quenneville et al., 2011). However, this approach only scales the yield stress and fails to capture the strain-rate sensitivity observed in elastic (pre-yield) and plastic (post-yield) regions of bone behavior (Hansen et al., 2008).

FE models based on subject-specific anatomically accurate geometries are widely utilized to study the biomechanical response of pedestrians involved in pedestrian-vehicle incidents and are gaining traction in forensic science applications (Li et al., 2013). Numerous studies suggest that subject-specific material property assignment increases the accuracy of the material models (Eberle et al., 2013; Goin et al., 2020). The existing strain-rate-dependent models lack subject-specific geometry and material property assignment (Cronin et al., 2022; Iwamoto et al., 2005). This study aims to develop a strain-rate-dependent material model for the human tibia that incorporates subject-specific anatomical geometry and material properties while capturing strain-rate sensitivity in pre- and post-yield regions. This model will be evaluated against the experimental data obtained from three-point bending tests on human tibias and will predict the structural response of the tibia over a range of impact velocities.

## METHODS

Figure 1 illustrates the methodology for developing the strain-rate-dependent material model. The strain-rate-dependent material model was developed through experimental testing combined with the inverse FE characterization method. Bending is the primary loading mode experienced by the tibia during vehicle-pedestrian collisions (Untaroiu et al., 2007). Previous researchers have performed three-point bending experiments on the tibia to understand the bone's response under car-pedestrian crashes (Cameron et al., 2020; Mo et al., 2012; Untaroiu et al., 2007). Therefore, human tibia specimens were subjected to dynamic three-point bend testing to replicate vehicle-pedestrian crashes utilizing a drop tower apparatus. The subject-specific finite element (SSFE) mesh for each specimen was generated using CT scan data, with heterogeneous



*This paper is a student paper from the 20th Injury Biomechanics Symposium and is published in a special issue of SAE International Journal of Transportation Safety.*
*It is preliminary work, has not been peer reviewed, and should not be cited because it is a work in progress.*

material properties assigned based on the distribution of Hounsfield numbers. A bilinear elastic-plastic strain-rate-dependent model was used to incorporate the strain-rate dependency for the cortical bone. A genetic algorithm-based inverse characterization method was used to optimize a single set of material parameters to reproduce the experimental force response from tests at impact velocities ranging from 1.5 to 5.0 m/s. The objective was to minimize the error between the simulation and experimental force-time response. The optimized material model was obtained based on its effectiveness in simulating the dynamic response of the bone.

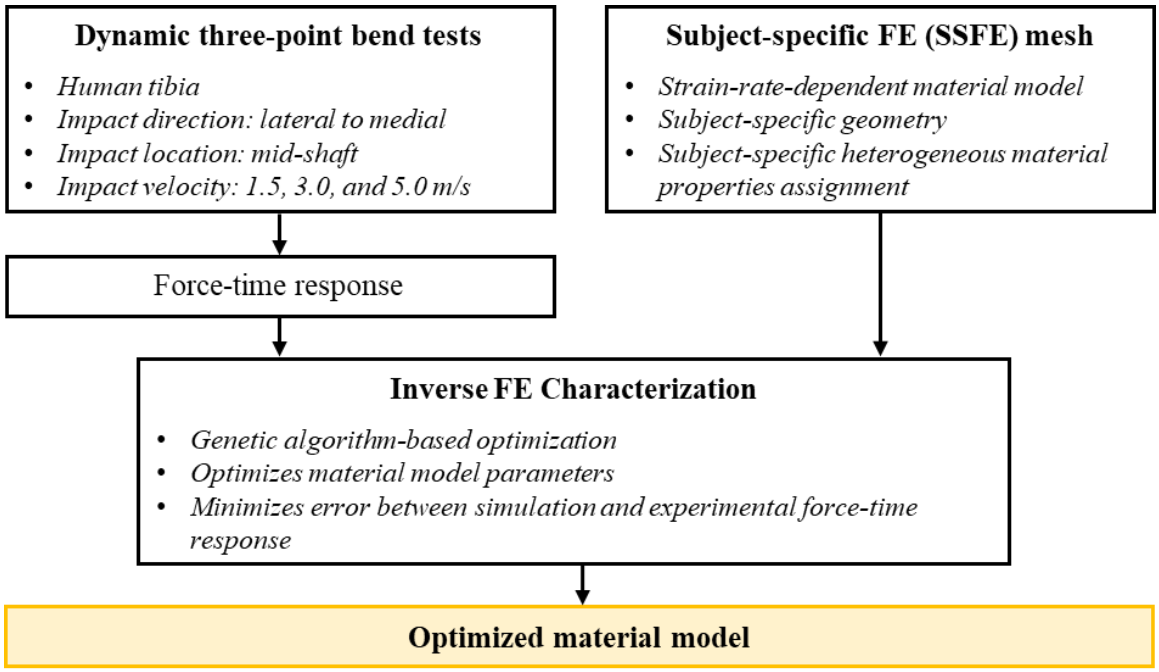


Figure 1: Methodology for developing a strain-rate-dependent material model.

## Experimental Testing

Three human tibias were obtained from un-embalmed post-mortem human subjects (PMHS) aged 40–60 years from the All India Institute of Medical Sciences (AIIMS) and Jai Prakash Narayan Apex Trauma Centre, New Delhi, India, following approval from their standing ethics committee. Specimens were wrapped in a thin polyethylene sheet, placed in an airtight container, and stored in a deep freezer at -20 °C. Before testing, specimens were thawed to room temperature, and all soft tissues were removed, as illustrated in Figure 2. Attention was focused on the bone ends, which were utilized to ensure the fixed orientation of the bone during the experiment. Additionally, special care was taken to prevent bone damage and to create artificial stress concentrators. Specimens were routinely sprayed with a 0.9% W/V saline solution to prevent dehydration.

Both bone extremities were potted in hollow aluminum mounts using quick-setting bone cement (Poly-Methyl Methacrylate, PMMA) to prevent the rotation of the bone from the intended test direction. A custom-built fixture facilitated the potting procedure. Before the potting



*This paper is a student paper from the 20th Injury Biomechanics Symposium and is published in a special issue of SAE International Journal of Transportation Safety.*
*It is preliminary work, has not been peer reviewed, and should not be cited because it is a work in progress.*

procedure, the mid-shaft of the specimens was wrapped in cotton gauze and sprayed with a 0.9% W/V saline solution to prevent dehydration resulting from heat produced during the curing of bone cement. The bone specimen was initially secured in the fixture in a predetermined orientation and alignment. The bone specimen was clamped in the fixture for 30 minutes to allow for the setting of the bone cement. The human tibia specimen (as shown in Figure 3) was oriented such that the impact direction was from lateral to medial (L–M), with the top surface in a relatively horizontal position facing the indenter.

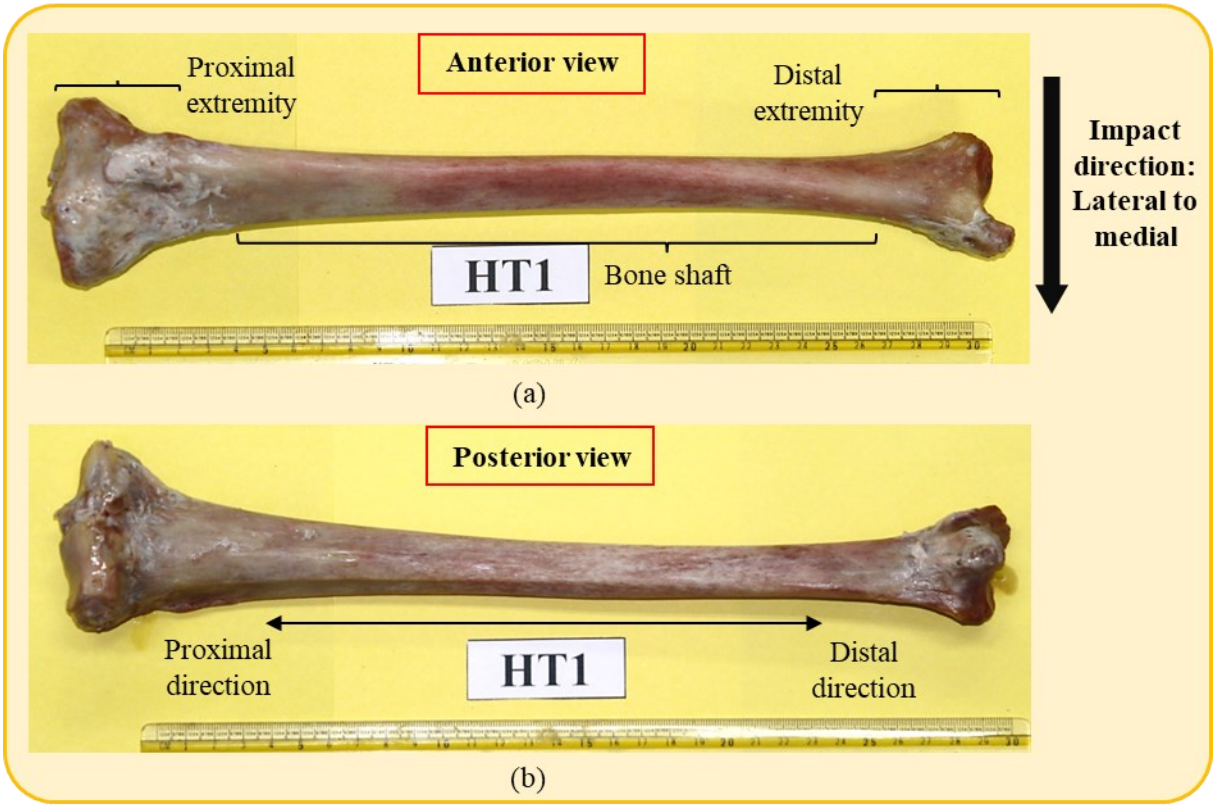


Figure 2: Anatomy of human tibia after soft tissue removal: (a) Anterior view, and (b) Posterior view.

All the bones were scanned before and after the potting using a micro-CT scanner (Scanco XtremeCT II™, Scanco Medical AG, Switzerland). The micro-CT scanner was calibrated with a standardized hydroxyapatite phantom (Q1 Scanco phantom with probes of 0, 100, 200, 400, and 800 mgHA). The CT scan data were used to develop subject-specific finite element (SSFE) models and to determine the specimens' geometric properties.

Dynamic three-point bend tests were performed utilizing a custom-built drop tower apparatus (Arun et al., 2011), illustrated in Figure 3. A piezoelectric load cell (Dytran 1053V6, Hottinger Brüel & Kjaer, United Kingdom) is fixed between the crosshead and the impactor to measure the load during the impact event. The data acquisition system (National Instruments, USB 6356) records the load-time history at a sampling rate of 20 kHz. The load-time history data were filtered using a Butterworth low-pass filter with a cutoff frequency of 1000 Hz to eliminate high-



*This paper is a student paper from the 20th Injury Biomechanics Symposium and is published in a special issue of SAE International Journal of Transportation Safety.*
*It is preliminary work, has not been peer reviewed, and should not be cited because it is a work in progress.*

frequency components. The load was applied using an impactor, a 20 mm semi-cylindrical steel rod, with the cylindrical side of the rod impacting the surface of the bone. The potted tibia specimens were positioned freely on the cylindrical roller support fixtures with a bending span of 200 mm, as illustrated in Figure 3. The specimens were impacted at the mid-shaft (impactor weight 30.5 kg) at velocities of 1.5, 3.0, and 5.0 m/s in the lateral to medial direction until failure. A high-speed digital camera (MotionPro® Y-Series) was used to record the displacement of the impactor and crack propagation at 20,000 frames per second. An external triggering mechanism was employed using a thin copper tape to initiate and synchronize the data acquisition system and high-speed digital camera recording.

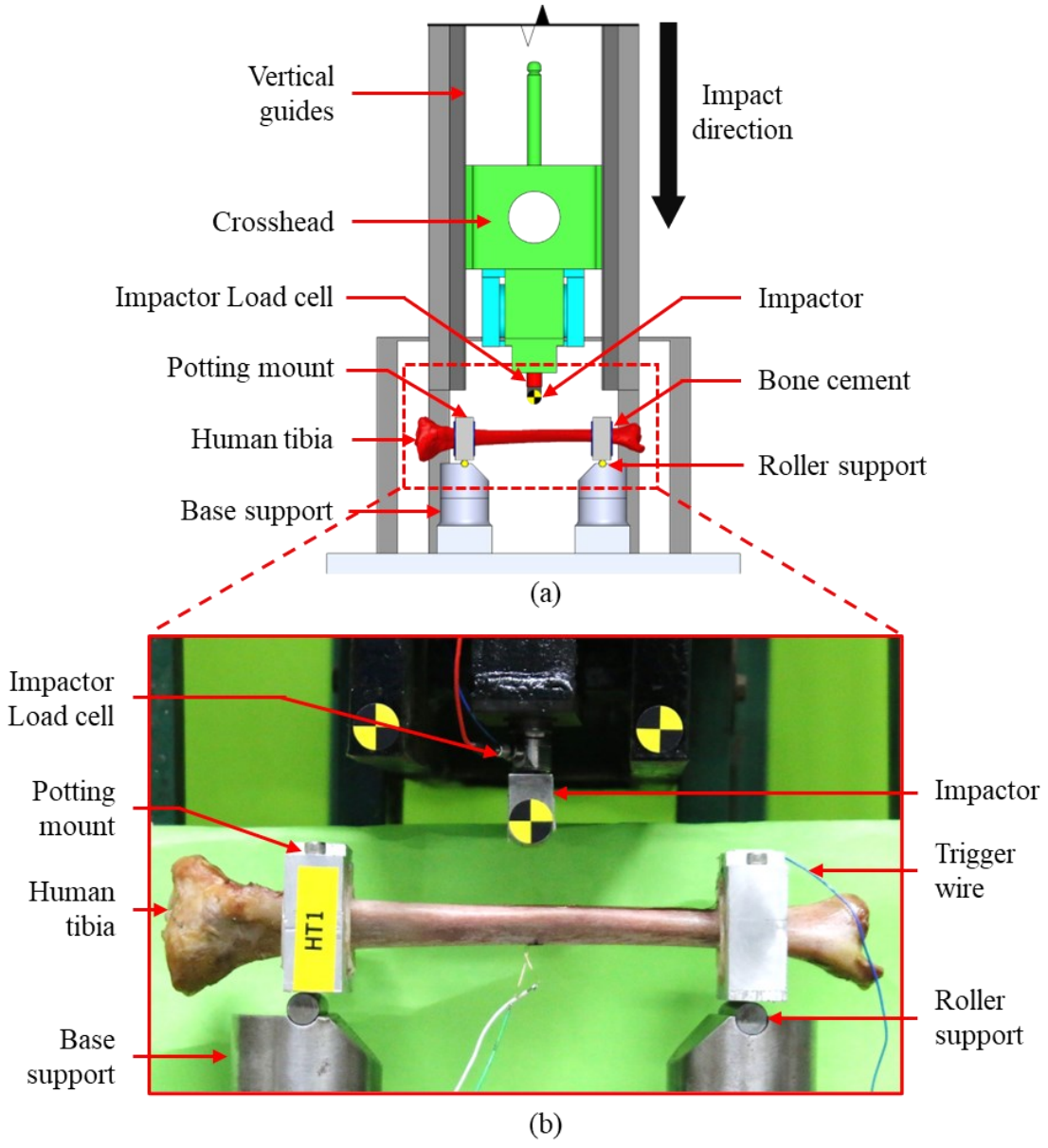


Figure 3: (a) Illustration of the custom-built drop tower apparatus for performing dynamic three-point bend tests; (b) three-point bend tests on human tibia.



*This paper is a student paper from the 20th Injury Biomechanics Symposium and is published in a special issue of SAE International Journal of Transportation Safety.*
*It is preliminary work, has not been peer reviewed, and should not be cited because it is a work in progress.*

**Subject-specific FE Modeling**

CT scans of the human tibia were analyzed utilizing Mimics® 24.0 (Materialise, Leuven, Belgium). The grayscale threshold filter was employed for the initial segmentation. Manual editing, region growing, and erasing tools were used to refine the segmented model carefully. Following the development of the surface mesh, HyperMesh (v. 2022, Altair Engineering, Inc., USA) was utilized to produce a tetrahedral volumetric mesh, which was subsequently refined.

The volumetric SSFE models were imported into Mimics to assign isotropic heterogeneous material properties. The isotropic heterogeneous material properties were assigned based on grey-scale information obtained from CT scan data, as shown in Figure 4. The standardized hydroxyapatite phantom (Q1 Scanco phantom) was used to establish a linear relationship between Hounsfield units (HU) and bone apparent density (ρ). Bone apparent density was divided into 100 separate material bins according to the HU values (Malik et al., 2023). To reproduce the experimental configuration, SSFE models were initially exported to HyperMesh and subsequently imported into the LS-DYNA™ solver, where boundary conditions were defined for performing finite element (FE) simulations (the model is seen in Figure 5).

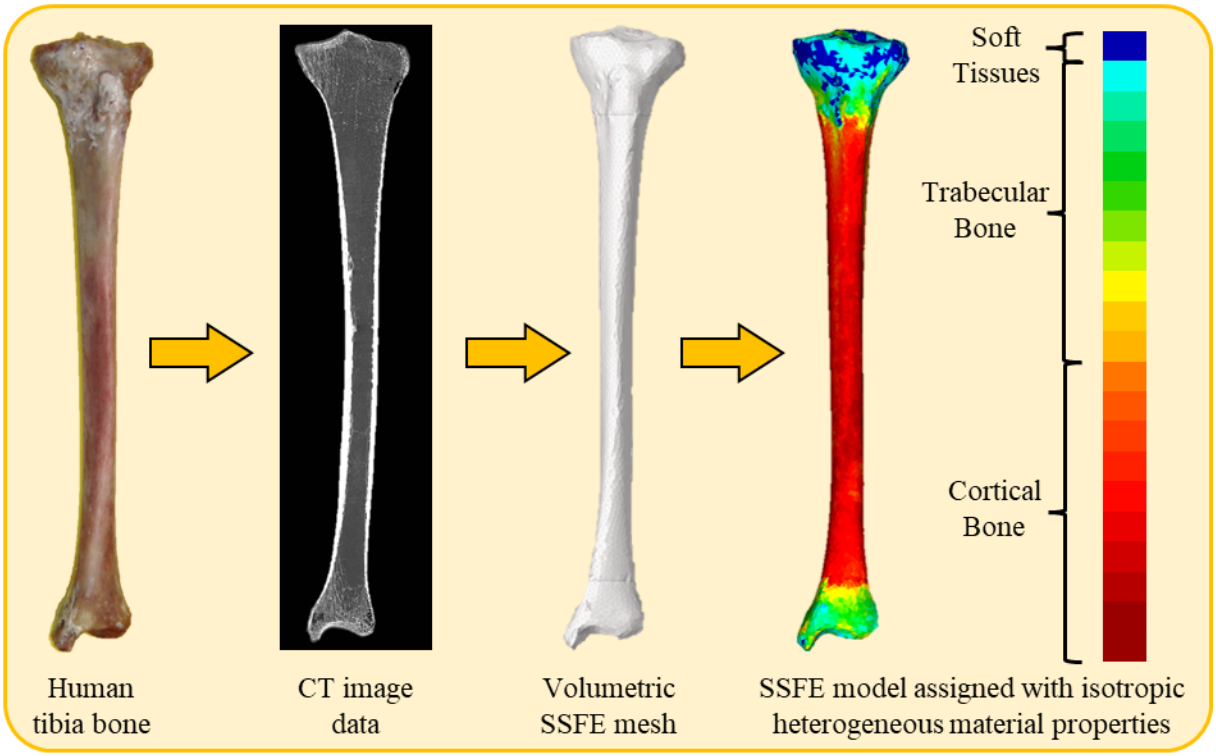


Figure 4: Heterogeneous material properties assigned to volumetric SSFE models.

The roller supports, aluminum mounts, bone cement, and impactor were modeled as rigid materials with tetrahedral elements to minimize computational demand. The impactor and roller supports were specifically modeled due to their significant influence on the dynamic response, which cannot be captured through a set of constraints (Arun et al., 2013). The SSFE model of bone



*This paper is a student paper from the 20th Injury Biomechanics Symposium and is published in a special issue of SAE International Journal of Transportation Safety.*
*It is preliminary work, has not been peer reviewed, and should not be cited because it is a work in progress.*

rested freely on the roller supports, with reference to post-potting CT images to replicate the experimental configuration. The impactor was given an initial velocity based on the high-speed camera experimental data along the impact direction (-'Z' in the model axis) and constrained to translate in the 'Z' direction. The roller supports were restricted in all degrees of freedom, while the bone, aluminum mounts, and bone cement were unconstrained. AUTOMATIC_SURFACE_TO_SURFACE contact simulated the interaction between the impactor and bone. In the post-processing, the contact force between the bone and impactor along the impact direction ('Z' direction) was obtained at a frequency of 20 kHz and used in the inverse FE characterization method. Simulation force-time response data was processed similarly to the experimental data.

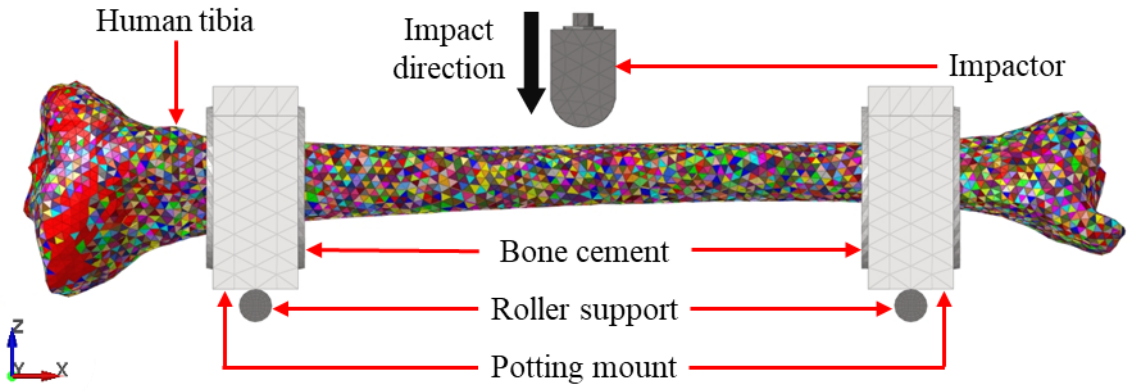


Figure 5: SSFE model replicating the human tibia's dynamic three-point bend test.

For finite elements in each bin, the quasi-static elastic modulus ($E_0$, GPa) and quasi-static yield stress ($\sigma_{y0}$, GPa) were mapped using the power law relationships (Equations 1 and 2) by the assigned bin's average $\rho$ (g/cm$^3$) value.

$$E_0 = a\rho^b \quad (1)$$

$$\sigma_{y0} = c\rho^d \quad (2)$$

Where $a$, $b$, $c$, and $d$ represent material parameters determined through the inverse FE characterization approach.

This work used a bilinear elastic-plastic material to model trabecular bone. The preliminary parametric sensitivity analysis suggests that trabecular bone has no significant effect on the dynamic response of bone during three-point bending. Consequently, the material properties (Table 1) were derived from (Linde et al., 1989). The strain-rate-dependent material model was used only to model the cortical bone, and its parameters were determined through the inverse FE characterization method.



*This paper is a student paper from the 20th Injury Biomechanics Symposium and is published in a special issue of SAE International Journal of Transportation Safety.*
*It is preliminary work, has not been peer reviewed, and should not be cited because it is a work in progress.*

Table 1: Material properties of trabecular bone

| **LS-DYNA Material Model:** MAT_PIECEWISE_LINEAR_PLASTICITY (MAT_24) | | | | |
|---|---|---|---|---|
| **Young's modulus (GPa)** | **Poisson's ratio** | **Yield stress (GPa)** | **Tangent modulus (GPa)** | **Cowper-Symonds model parameters** |
| 0.445 | 0.3 | 0.0053 | 0 | C = 0<br>P = 0 |

**Strain-rate-dependent Material Model**

The existing elastic-plastic constitutive model (MAT_24) in LS-DYNA™ uses Cowper-Symonds model parameters to account for strain-rate effects only in yield stress. However, cortical bone's pre- and post-yield behavior was also known to exhibit strain-rate dependency (Hansen et al., 2008; Johnson et al., 2010), which was not considered in the Cowper-Symonds model. Therefore, a bilinear elastic-plastic material model incorporating strain-rate dependency in both the pre- and post-yield regimes was implemented using a user-defined material subroutine (UMAT) in LS-DYNA™. Figure 6 illustrates a schematic representation of this bilinear elastic-plastic strain-rate-dependent model.

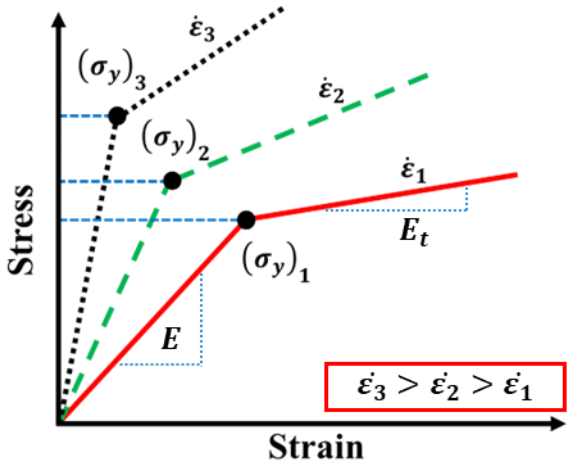


Figure 6: A schematic showing strain-rate-dependent material model.

In this study, the fracture phenomenon of bone was not considered; thus, only the pre-fracture behavior was modeled, and simulations were conducted until fracture was observed in the tests. This strain-rate-dependent model incorporates the strain-rate dependence of elastic modulus, yield stress, and tangent modulus. For each element, quasi-static elastic modulus ($E_0$) and yield stress ($\sigma_{y0}$) were mapped using the power law relationships by the assigned $\rho$ value (Equations 1 and 2). Strain-rate dependency was incorporated in previous studies using exponential, logarithmic, and polynomial functions (Arun et al., 2011; Enns-Bray et al., 2018; Li et al., 2020). In this study, a combined exponential and logarithmic function (Equations 3 and 4) was used to obtain the strain-rate-dependent elastic modulus ($E$) and yield stress ($\sigma_y$), respectively. Strain-rate-dependent parameters were scaled based on the quasi-static strain rate ($\dot{\varepsilon}_0$) and the target strain



*This paper is a student paper from the 20th Injury Biomechanics Symposium and is published in a special issue of SAE International Journal of Transportation Safety.*
*It is preliminary work, has not been peer reviewed, and should not be cited because it is a work in progress.*

rate ($\dot{\varepsilon}$). In Equations 3 and 4, $B_1$ and $B_2$ are material parameters determined using the inverse FE characterization method. A von Mises criterion was used to capture yielding. Equation 5 was used to determine the tangent modulus ($E_t$), which was calculated as a factor "$t$" times the strain-rate-dependent elastic modulus ($E$). As listed in Table 2, seven material properties were optimized using the inverse FE characterization method.

$$E = \frac{1}{2}E_0\left(1 + B_1{}^{log\left(\frac{\dot{\varepsilon}}{\dot{\varepsilon}_0}\right)}\right) \quad (3)$$

$$\sigma_y = \frac{1}{2}\sigma_{y0}\left(1 + B_2{}^{log\left(\frac{\dot{\varepsilon}}{\dot{\varepsilon}_0}\right)}\right) \quad (4)$$

$$E_t = t * E \quad (5)$$

Table 2: Material parameters optimized using inverse FE characterization

| **Material properties** | **Equation** | **Material parameters** |
|---|---|---|
| Quasi-static elastic modulus ($E_0$) | $E_0 = \boldsymbol{a}\rho^{\boldsymbol{b}}$ | $a$ & $b$ |
| Strain-rate-dependent elastic modulus ($E$) | $E = \frac{1}{2}E_0\left(1 + \boldsymbol{B_1}{}^{log\left(\frac{\dot{\varepsilon}}{\dot{\varepsilon}_0}\right)}\right)$ | $B_1$ |
| Quasi-static yield stress ($\sigma_{y0}$) | $\sigma_{y0} = \boldsymbol{c}\rho^{\boldsymbol{d}}$ | $c$ & $d$ |
| Strain-rate-dependent yield stress ($\sigma_y$) | $\sigma_y = \frac{1}{2}\sigma_{y0}\left(1 + \boldsymbol{B_2}{}^{log\left(\frac{\dot{\varepsilon}}{\dot{\varepsilon}_0}\right)}\right)$ | $B_2$ |
| Tangent modulus ($E_t$) | $E_t = \boldsymbol{t} \times E$ | $t$ |

**Inverse FE Characterization**

Inverse FE characterization is an iterative process that employs optimization methods to adjust material characteristics to reduce the variation between experimental and simulated force data. This study utilized inverse FE characterization based on the genetic algorithm (GA) optimization technique, as seen in Figure 7, and implemented it using MATLAB's GA toolbox (version R2022b, MathWorks, Inc.). GA optimization is a heuristic search technique derived from the principles of natural selection. The initial population was created within the specified range of material parameters (Table 3) and is evaluated using an objective function that quantifies its effectiveness in solving the problem. If the convergence criteria are unsatisfied, a new population is generated from the more successful members of the previous population through selection, crossover, and mutation operations. The new generation substitutes the old; this cycle continues until the convergence conditions are satisfied. The population gradually advances towards optimal solutions, converging on the optimal material parameters.



*This paper is a student paper from the 20th Injury Biomechanics Symposium and is published in a special issue of SAE International Journal of Transportation Safety.*
*It is preliminary work, has not been peer reviewed, and should not be cited because it is a work in progress.*

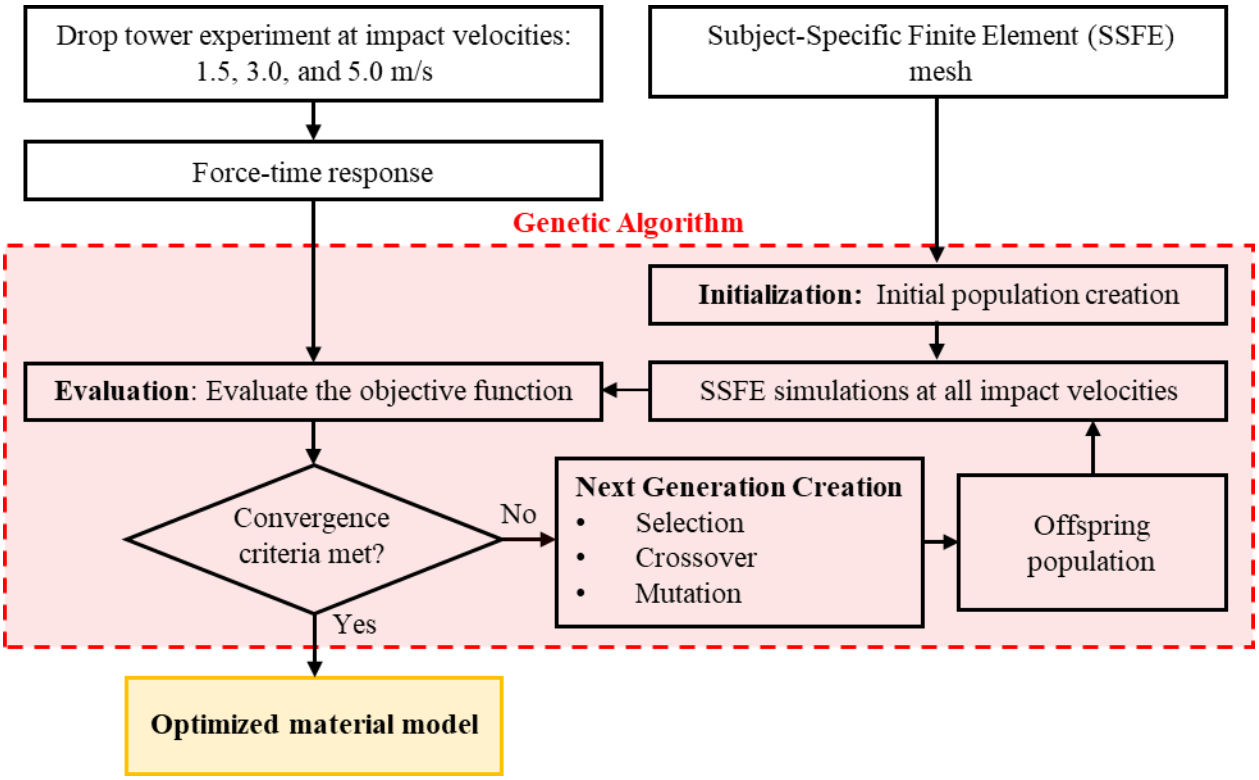


Figure 7: Flowchart of genetic algorithm-based inverse FE characterization methodology.

The variation between the experimental and SSFE force-time responses (Equation 6) for individual impact velocity was determined using a normalized root mean square error function ($NRMS^j$).

$$NRMS^j = \sqrt{\frac{1}{n^j}\sum_{i=1}^{n^j}\left(\frac{F_i^{fem,j} - F_i^{exp,j}}{max.(F_i^{exp,j})}\right)^2}, \forall j = 1\ to\ 3 \qquad (6)$$

Where the $F_i^{exp,j}$ and $F_i^{fem,j}$ are the experimental and FE force values corresponding to the individual impact velocity ($j$); the index $j$ corresponds to the different impact velocities (1.5, 3.0, and 5.0 m/s); and $n_j$ is the number of data points according to the corresponding test. The root mean square error function is normalized using the maximum experimental force value ($max.(F_i^{exp,j})$) corresponding to the specific impact velocity. The objective of the GA was to minimize the summation of uniformly weighted $NRMS$ values for all individual velocities, as expressed in Equation 7.

$$\text{Objective function, } f: \ min\ NRMS^{total} = \sum_{j=1}^{3} NRMS^j \qquad (7)$$

A single set of optimized material model parameters was obtained to reproduce the force response from 1.5 to 5.0 m/s. The material parameters and their range used in the overall optimization study are presented in Table 3.



*This paper is a student paper from the 20th Injury Biomechanics Symposium and is published in a special issue of SAE International Journal of Transportation Safety.*
*It is preliminary work, has not been peer reviewed, and should not be cited because it is a work in progress.*

## RESULTS

This study successfully tested three cadaveric human tibia samples under dynamic three-point bend loading. Figure 8 shows that the peak load at failure increased monotonically with impact velocity and was 1.9, 4.04, and 5.1 kN for 1.5, 3.0, and 5.0 m/s, respectively. The time for fracture initiation diminished with increasing velocity, recorded as 3.15, 2.15, and 0.9 ms. The initial force-time slope exhibited a velocity-dependent pattern, reaching a maximum of 7.89 kN/ms at 5.0 m/s and declining to 1.26 kN/ms at 1.5 m/s. Oblique fractures were observed in all tests.

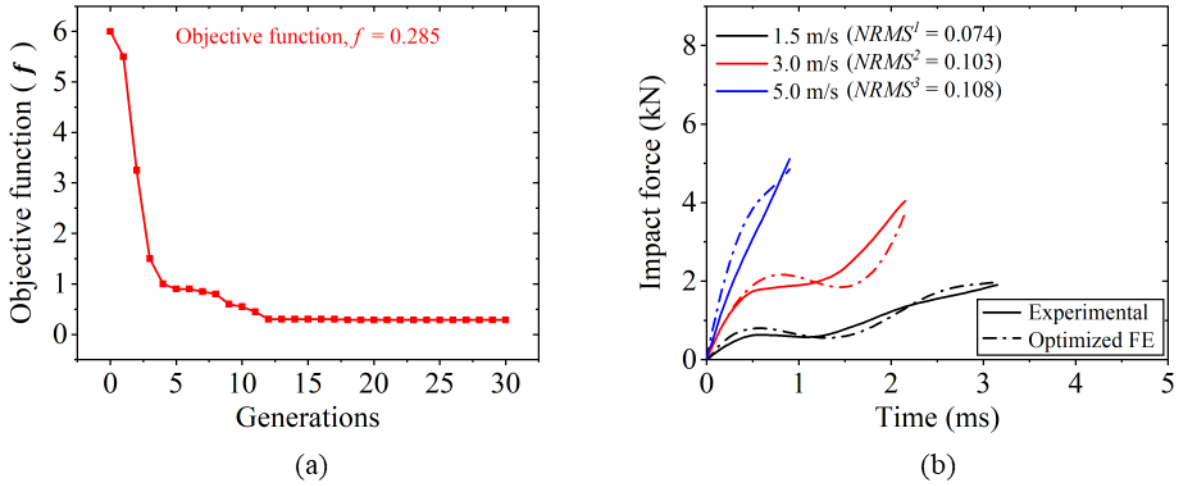


Figure 8: (a) GA Convergence plot; (b) Experimental and optimized force-time response.

Experimental force-time data and SSFE models were used as inputs in the inverse finite element characterization approach to optimize material parameters by minimizing the objective function (Equation 7). The convergence of the objective function (Figure 8) was achieved by the 12$^{th}$ iteration, with a minor decline observed at the 18$^{th}$ iteration (objective function value: 0.285). The computational and experimental force-time response (Figure 8) correlate reasonably well ($NRMS$ errors: 0.074, 0.103, and 0.108 for 1.5, 3.0, and 5.0 m/s, respectively). Table 3 lists the optimized material parameters. The quasi-static elastic modulus of cortical bone varies from 7.75 GPa to 17.62 GPa, while the yield stress ranges from 59 MPa to 116 MPa.



*This paper is a student paper from the 20$^{th}$ Injury Biomechanics Symposium and is published in a special issue of SAE International Journal of Transportation Safety.*
*It is preliminary work, has not been peer reviewed, and should not be cited because it is a work in progress.*

Table 3: Range and optimized values of material parameters optimized using inverse FE characterization

| Material parameters | Range | | Optimized value |
|---|---|---|---|
| $a$ | 1.0 | 12 | 9.96 |
| $b$ | 0.1 | 2.5 | 0.88 |
| $B_1$ | 0.5 | 1.5 | 1.28 |
| $c$ | 0.01 | 0.1 | 0.073 |
| $d$ | 0.1 | 2.5 | 0.72 |
| $B_2$ | 0.5 | 1.5 | 1.13 |
| $t$ | 0.001 | 0.10 | 0.055 |

## DISCUSSION

The optimized quasi-static elastic modulus–density ($E_0 - \rho$) relationship derived in this present study was compared to previously known relations given in Table 4. In addition to the relation proposed by (Carter et al., 1977), we also employed the relations developed from measurements of human tibia specimens using mechanical (Schneider et al., 1991) and ultrasound (Rho et al., 1995) methods. Figure 9 shows that the optimized $E_0 - \rho$ relationship is somewhat a hybrid of Equations 8 and 9, whereas significant disagreement was observed with Equation 10. At lower $\rho$, the optimized elastic modulus is closer to Rho et al. (1995), while at higher $\rho$, the modulus is closer to Snyder et al. (1991). The optimized quasi-static yield stress–density ($\sigma_{y0} - \rho$) relationship was compared to relations (Table 5) based on the compression yield stress of human femur cortical bone (Keller, 1994) and rat femur cortical bone (Cory et al., 2010). To the best of the author's knowledge, $\sigma_{y0} - \rho$ relationship specific to the human tibia was not available in the literature. The optimal yield stress is larger than others at lower ρ, and following 1.4 g/cm$^3$, it lies between the two relationships (Figure 9). Disagreements with the optimized relationships are likely due to differences in mechanical testing procedures and bone sites. Thus, the quasi-static material parameters of the developed strain-rate-dependent model are reasonably aligned within the range of values established in prior studies.

Table 4: Elastic modulus–density relationships compared to the optimized relationship

| Reference | Bone Site | Relation | |
|---|---|---|---|
| Snyder and Schneider (1991) | Human tibial diaphysis | $E_0 = 3.891\rho^{2.39}$ | (8) |
| Rho et al., (1995) | Human tibia | $E_0 = 13\rho - 3.842$ | (9) |
| Carter and Hayes (1977) | Pooled | $E_0 = 3.79\rho^{3.0}$ | (10) |

Table 5: Yield stress–density relationships compared to the optimized relationship

| Reference | Bone Site | Relation | |
|---|---|---|---|
| Keller (1994) | Human femur cortical | $\sigma_{y0} = 0.0407\rho^{1.72}$ | (11) |
| Cory et al., 2010 | Rat femur cortical | $\sigma_{y0} = 0.0534\rho^{1.64}$ | (12) |



*This paper is a student paper from the 20th Injury Biomechanics Symposium and is published in a special issue of SAE International Journal of Transportation Safety.*
*It is preliminary work, has not been peer reviewed, and should not be cited because it is a work in progress.*

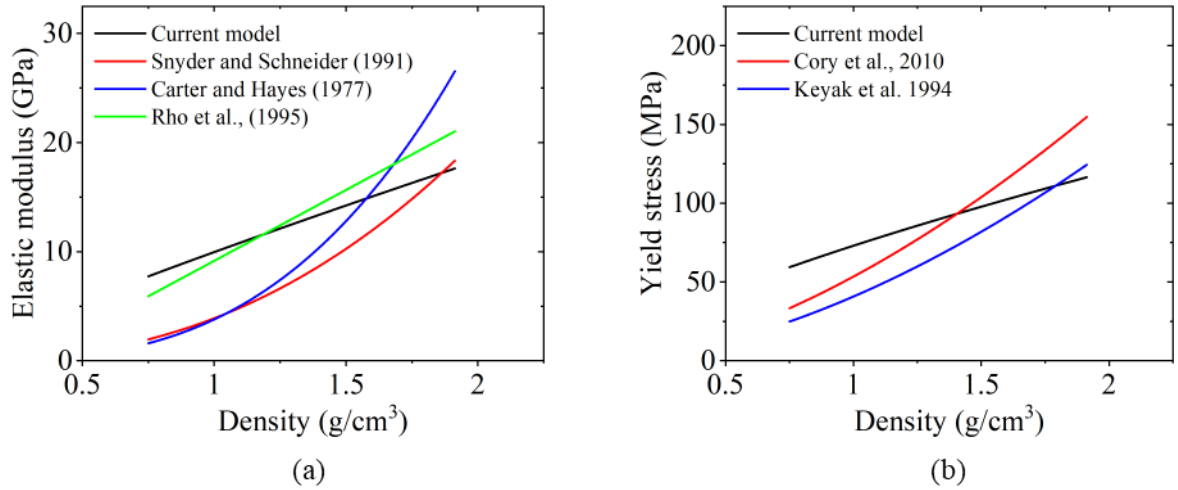


Figure 9: (a) Comparing elastic modulus–density relationships; (b) Comparing yield stress–density relationships.

Cortical bone material models employed by commonly used human body models, such as the Total Human Model for Safety (THUMS) and Global Human Body Models Consortium (GHBMC), were compared to the developed strain-rate-dependent material model (Figure 10). The corresponding material properties are detailed in Table 6 and 7. THUMS uses an elasto-plastic material model incorporating strain-rate effects via the Cowper-Symonds formulation. In contrast, GHBMC uses a strain rate-dependent material model that uses curves to define rate effects for yield stress, Young's modulus, and tangent modulus. The homogenous FE model based on the subject-specific geometry of the specimen impacted at 1.5 m/s was used for comparison. The optimized FE model developed in this study demonstrates better agreement with the experimental data, attaining a $NRMS$ of 0.074, in contrast to 0.106 for THUMS and 0.235 for GHBMC. This improvement suggests that employing a subject-specific finite element model integrated with a strain-rate-dependent material model improves the biofidelity of FE simulations of the tibial response under dynamic loading.

Table 6: THUMS cortical bone material model

| **Source:** THUMS: AM50 V7.1 Occupant | | | | | |
|---|---|---|---|---|---|
| **LS-DYNA Material Model:** MAT_PIECEWISE_LINEAR_PLASTICITY (MAT_24) | | | | | |
| **Density ($kg/m^3$)** | **Young's modulus (GPa)** | **Poisson's ratio** | **Yield stress (GPa)** | **Tangent modulus (GPa)** | **Cowper-Symonds model parameters** |
| 2000 | 18.0 | 0.3 | 0.0361 | 14.8 | C = 360.7<br>P = 4.605 |



*This paper is a student paper from the 20th Injury Biomechanics Symposium and is published in a special issue of SAE International Journal of Transportation Safety.*
*It is preliminary work, has not been peer reviewed, and should not be cited because it is a work in progress.*

Table 7: GHBMC cortical bone material model

| **Source:** GHBMC M50-P V1.5 | | | | | |
|---|---|---|---|---|---|
| **LS-DYNA Material Model:** MAT_STRAIN_RATE_DEPENDENT_PLASTICITY (MAT_19) | | | | | |
| **Density ($kg/m^3$)** | **Young's modulus (GPa)** | **Poisson's ratio** | **Yield stress (GPa)** | **Tangent modulus (GPa)** | **Strain-rate dependence** |
| 2000 | 17.5 | 0.3 | 0.125 to 0.198* | 1.0 | *using curves |
| *Defined using curves for the yield stress, Young's modulus, and tangent modulus versus the effective strain rate. | | | | | |

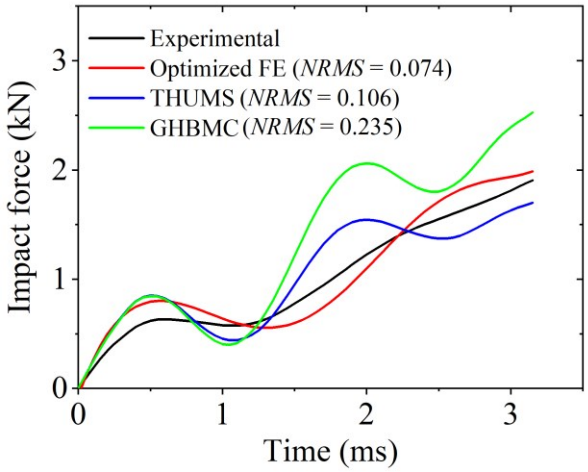


Figure 10: Force-time response comparison between experimental data, optimized FE model, THUMS, and GHBMC.

Although the optimized force-time response reasonably correlates with the experimental response, the possible reason for the mismatch of curves could be due to the current model's inability to incorporate the cortical bone's complex behavior. Cortical bone exhibits viscoelasticity, material anisotropy, and compression-tension asymmetric yielding (Cowin, 2001). The developed material model is an isotropic bilinear elastic-plastic material model with symmetric yielding applied using von Mises yield criteria. Previous studies have attempted to improve the predictive accuracy of finite element material models by incorporating various features of bone behavior across diverse bone specimens subjected to varying loading conditions (Derikx et al., 2011; Ün et al., 2016). The material model incorporating all bone features implemented on the dynamic behavior of bone could be pursued as future work.

## Limitations and Future Work

In this study, the fracture phenomenon is not modeled. Additionally, the current model does not effectively capture the complete behavior of cortical bones, including failure mechanisms, viscoelasticity, material orthotropy, and compression-tension asymmetry yielding. Therefore,



*This paper is a student paper from the 20th Injury Biomechanics Symposium and is published in a special issue of SAE International Journal of Transportation Safety.*
*It is preliminary work, has not been peer reviewed, and should not be cited because it is a work in progress.*

these concerns must be addressed in future material model developments while balancing computational efficiency and the number of material parameters. Furthermore, the above results are based on a single experiment at each impact velocity. Consequently, additional repetitions will be conducted in the future to ensure the material model's reliability.

## CONCLUSIONS

The structural response of the human tibia subjected to dynamic three-point bending loads was predicted in the current study. The experimental force-time response was used to optimize the strain-rate-dependent material model parameters using a genetic algorithm-based inverse FE characterization. The largest $NRMS$ error across all impact velocities was 0.108, indicating that the simulated results and the experimental load-time responses demonstrate a reasonable correlation. This study highlights the significance of employing a subject-specific finite element model integrated with a strain-rate-dependent material model to simulate the tibial response during pedestrian-vehicle collisions. Beyond pedestrian safety, the model can aid in forensic biomechanics (impact reconstructions), and its integration of subject-specific data also supports personalized injury risk assessment. Incorporating fracture initiation and propagation modeling, along with other complex bone behaviors, will necessitate further enhancements to the current material model. The improved FE material model of the tibia will aid in designing injury countermeasures for vehicle front-ends and improve our understanding of the injury mechanisms resulting from pedestrian-vehicle accidents. More repetitions will be conducted to ensure the model's reliability, as the current results are based on a single test at each velocity.

## ACKNOWLEDGEMENTS

The authors acknowledge the financial support received from the DRDO Industry Academia Centre of Excellence, IIT Delhi (DFTM/03/3203/M/01/JATC).

## REFERENCES

ABDEL-WAHAB, A. A., SILBERSCHMIDT, V. V. (2011). Dynamic properties of cortical bone tissue: Impact tests and numerical study. In Applied Mechanics and Materials (Vol. 70).

ABRAHAM, A. C., AGARWALLA, A., YADAVALLI, A., LIU, J. Y., TANG, S. Y. (2016). Microstructural and compositional contributions towards the mechanical behavior of aging human bone measured by cyclic and impact reference point indentation. Bone, 87, 37–43.



*This paper is a student paper from the 20th Injury Biomechanics Symposium and is published in a special issue of SAE International Journal of Transportation Safety.*
*It is preliminary work, has not been peer reviewed, and should not be cited because it is a work in progress.*

ARUN, M. W. J., CHAWLA, A., MUKHERJEE, S. (2011). Predicting fracture initiation, propagation and diversion in long bones under impact using Drucker-Prager plastic model and damage modeling. American Society of Biomechanics, 3: 56-64.

ARUN, M. W. J., MUKHERJEE, S., CHAWLA, A., SHARMA, G., SHAH, P., AGEORGES, C. (2013). Characterization of Human Long Bones Using Experiments, Imaging and Inverse Finite Element Techniques. The International Research Council on Biomechanics of Injury, 1: IRC-13-21.

ASGHARPOUR, Z., ZIOUPOS, P., GRAW, M., PELDSCHUS, S. (2014). Development of a strain rate dependent material model of human cortical bone for computer-aided reconstruction of injury mechanisms. Forensic Science International, 236, 109–116.

CAMERON, M. W., SCHEMITSCH, E. H., ZDERO, R., QUENNEVILLE, C. E. (2020). Biomechanical impact testing of synthetic versus human cadaveric tibias for predicting injury risk during pedestrian-vehicle collisions. Traffic Injury Prevention, 21(2), 163–168.

CARTER, D. R., HAYES, W. C. (1977). The compressive behavior of bone as a two-phase porous structure. Journal of Bone and Joint Surgery - Series A, 59(7), 954–962.

CORY, E., NAZARIAN, A., ENTEZARI, V., VARTANIANS, V., MÜLLER, R., SNYDER, B. D. (2010). Compressive axial mechanical properties of rat bone as functions of bone volume fraction, apparent density and micro-ct based mineral density. Journal of Biomechanics, 43(5), 953–960.

COWIN, S. C. (2001). Bone mechanics handbook, second edition. In Bone Mechanics Handbook, Second Edition. CRC Press.

CRONIN, D. S., WATSON, B., KHOR, F., GIERCZYCKA, D., & MALCOLM, S. (2022). Cortical bone continuum damage mechanics constitutive model with stress triaxiality criterion to predict fracture initiation and pattern. Frontiers in Bioengineering and Biotechnology, 10(October), 1–15.

DERIKX, L. C., VIS, R., MEINDERS, T., VERDONSCHOT, N., TANCK, E. (2011). Implementation of asymmetric yielding in case-specific finite element models improves the prediction of femoral fractures. Computer Methods in Biomechanics and Biomedical Engineering, 14(2), 183–193.

EBERLE, S., GÖTTLINGER, M., AUGAT, P. (2013). An investigation to determine if a single validated density-elasticity relationship can be used for subject specific finite element analyses of human long bones. Medical Engineering and Physics, 35(7), 875–883.

ENNS-BRAY, W. S., BAHALOO, H., FLEPS, I., ARIZA, O., GILCHRIST, S., WIDMER, R., GUY, P., PÁLSSON, H., FERGUSON, S. J., CRIPTON, P. A., HELGASON, B. (2018). Material mapping strategy to improve the predicted response of the proximal femur to a



*This paper is a student paper from the 20th Injury Biomechanics Symposium and is published in a special issue of SAE International Journal of Transportation Safety.*
*It is preliminary work, has not been peer reviewed, and should not be cited because it is a work in progress.*

sideways fall impact. Journal of the Mechanical Behavior of Biomedical Materials, 78(September 2017), 196–205.

FLEPS, I., GUY, P., FERGUSON, S. J., CRIPTON, P. A., HELGASON, B. (2019). Explicit Finite Element Models Accurately Predict Subject-Specific and Velocity-Dependent Kinetics of Sideways Fall Impact. Journal of Bone and Mineral Research, 34(10), 1837–1850.

GOIN, B., RENAULT, J. B., THIBES, L., CHABRAND, P. (2020). Influence of material properties and boundary conditions on patient-specific models. Computer Methods in Biomechanics and Biomedical Engineering, 24(4), 429–439.

HANSEN, U., ZIOUPOS, P., SIMPSON, R., CURREY, J. D., HYND, D. (2008). The effect of strain rate on the mechanical properties of human cortical bone. Journal of Biomechanical Engineering, 130(1), 1–8.

IWAMOTO, M., MIKI, K., & TANAKA, E. (2005). Ankle Skeletal Injury Predictions Using Anisotropic Inelastic Constitutive Model of Cortical Bone Taking into Account Damage Evolution. SAE Technical Papers, 2005-November, 133–156.

JOHNSON, T. P. M., SOCRATE, S., BOYCE, M. C. (2010). A viscoelastic, viscoplastic model of cortical bone valid at low and high strain rates. Acta Biomaterialia, 6(10), 4073–4080.

KELLER, T. S. (1994). Predicting the compressive mechanical behavior of bone. Journal of Biomechanics, 27(9), 1159–1168.

LI, Z., WANG, J. J. J., WANG, J. J. J., WANG, J. J. J., JI, C., WANG, G. (2020). Experimental and numerical study on the mechanical properties of cortical and spongy cranial bone of 8-week-old porcines at different strain rates. Biomechanics and Modeling in Mechanobiology, 19(5), 1797–1808.

LI, Z., ZOU, D., LIU, N., ZHONG, L., SHAO, Y., WAN, L., HUANG, P., CHEN, Y. (2013). Finite element analysis of pedestrian lower limb fractures by direct force: The result of being run over or impact? Forensic Science International, 229(1–3), 43–51.

LINDE, F., HVID, I., PONGSOIPETCH, B. (1989). Energy absorptive properties of human trabecular bone specimens during axial compression. Journal of Orthopaedic Research, 7(3), 432–439.

MALIK, A., YADAV, V. V., CHAWLA, A., DATLA, N. V. (2023). Predicting Impact Response of Human Femur using Material Mapping Strategy. 28th Congress of the European Society of Biomechanics.

MO, F., ARNOUX, P. J., JURE, J. J., MASSON, C. (2012). Injury tolerance of tibia for the car-pedestrian impact. Accident Analysis and Prevention, 46, 18–25.



*This paper is a student paper from the 20th Injury Biomechanics Symposium and is published in a special issue of SAE International Journal of Transportation Safety.*
*It is preliminary work, has not been peer reviewed, and should not be cited because it is a work in progress.*

QUENNEVILLE, C. E., DUNNING, C. E. (2011). Development of a finite element model of the tibia for short-duration high-force axial impact loading. Computer Methods in Biomechanics and Biomedical Engineering, 14(2), 205–212.

RHO, J. Y., HOBATHO, M. C., ASHMAN, R. B. (1995). Relations of mechanical properties to density and CT numbers in human bone. Medical Engineering and Physics, 17(5), 347–355.

SCHNEIDER, E., SNYDER, M. (1991). Estimation of Mechanical Properties of Cortical Bone by Computed Tomography. Journal of Orthopaedic Research, 9(17), 422–431.

SINGARAM, S., NAIDOO, M. (2019). The physical, psychological and social impact of long bone fractures on adults: A review. African Journal of Primary Health Care and Family Medicine, 11(1).

ÜN, K., ÇALIK, A. (2016). Relevance of inhomogeneous–anisotropic models of human cortical bone: a tibia study using the finite element method. Biotechnology and Biotechnological Equipment, 30(3), 538–547.

UNTAROIU, C., KERRIGAN, J., KAM, C., CRANDALL, J., YAMAZAKI, K., FUKUYAMA, K., KAMIJI, K., YASUKI, T., FUNK, J. (2007). Correlation of Strain and Loads Measured in the Long Bones with Observed Kinematics of the Lower Limb during Vehicle-Pedestrian Impacts. SAE Technical Papers, 2007-October.

WHO. (2023). Global status report on road safety 2023. In World Health Organization, Geneva, Switzerland (Vol. 15, Issue 4).

YANG, J. (2005). Review of injury biomechanics in car-pedestrian collisions. International Journal of Vehicle Safety, 1(1–3), 100–117.



*This paper is a student paper from the 20th Injury Biomechanics Symposium and is published in a special issue of SAE International Journal of Transportation Safety.*
*It is preliminary work, has not been peer reviewed, and should not be cited because it is a work in progress.*